ELSEVIER

Aerospace Science and Technology 6 (2002) 435–449

Aerospace Science and Technology

www.elsevier.com/locate/aescte

A real-time kinematic GPS sensor for spacecraft relative navigation

Ein GPS Sensor zur kinematischen Relativnavigation von Raumfahrzeugen in Echtzeit

Oliver Montenbruck [a,*], Takuji Ebinuma [b], E. Glenn Lightsey [b], Sunny Leung [a]

[a] *German Space Operations Center, Deutsches Zentrum für Luft- und Raumfahrt, 82230 Weßling, Germany*
[b] *Center for Space Research, University of Texas, 3925 W. Braker Lane, Austin, TX 78759, USA*

Received 8 April 2002; received in revised form 19 June 2002; accepted 30 July 2002

Abstract

The concept and prototype implementation of a spaceborne relative navigation sensor based on a pair of GPS receivers is presented. It employs two individual receivers exchanging raw measurements via a dedicated serial data link. Besides computing their own navigation solution, the receivers process single difference measurements to obtain their mutual relative state. The differential processing provides a high level of common error cancellation while the resulting noise is minimized by appropriate use of carrier phase measurements. A prototype relative navigation sensor making use of the above concepts has been built up based on the GPS Orion 12 channel L1 receiver and qualified in hardware-in-the-loop tests using a GPS signal simulator. It provides a relative navigation solution with representative r.m.s. accuracies of 0.5 m and 1 cm/s, respectively, for position and velocity. For ease of use the relative state is provided in a co-moving frame aligned with the radial, cross-track and along-track direction. The purely kinematic nature of state estimation and the small latency make the system well suited for maneuvering spacecraft, while the minimalist hardware requirements facilitate its use on microsatellite formations.

Zusammenfassung

Die vorliegende Arbeit stellt das Konzept und die Prototypimplementierung eines raumgestützten Relativnavigationssensors vor, der auf einem Paar von GPS Empfängern basiert. Es werden zwei separate Empfänger eingesetzt, die Rohmessungen über eine dedizierte serielle Schnittstelle austauschen. Neben der Berechnung der eigenen Navigationslösung prozessieren die Empfänger Einfachdifferenzen dieser Messungen, um gegenseitig ihre Relativposition und Geschwindigkeit zu bestimmen. Die differentielle Prozessierung gewährleistet dabei in hohem Maß die Auslöschung gemeinsamer Fehleranteile, während der Rauschanteil durch die geeignete Nutzung von Trägerphasenmessungen minimiert wird. Der Prototyp eines derartigen Relativnavigationssensors wurde auf Basis eines GPS Orion 12 Kanal L1 Einfrequenzempfängers aufgebaut und mit Hilfe eines GPS Signalssimulators getestet. Er liefert eine Relativnavigationslösung mit repräsentativen Genauigkeiten von 0.5 m und 1 cm/s für Position und Geschwindigkeit. Zum einfachen Gebrauch wird die Relativnavigationslösung in einem mitbewegten Koordinatensystem dargestellt, das entlang der radialen Richtung, der Vorwärtsrichtung und der Bahnnormalen orientiert ist. Die rein kinematische Natur der Zustandsschätzung und die geringe Latenzzeit machen das System gut geeignet für Raumfahrzeuge mit aktivem Antrieb. Zusätzlich erleichtern die minimalistischen Hardwarevoraussetzungen den Einsatz in Formationen von Mikrosatelliten.

Keywords: Relative navigation; GPS; Formation flying; Rendezvous & docking; Orion

Schlüsselwörter: Relativnavigation; GPS; Formationsflug; Rendezvous & docking; Orion

1. Introduction

Formation flying of satellites as well as proximity operations during rendezvous and docking require a precise knowledge of the relative state of the involved spacecraft. The potential of the Global Positioning System (GPS) for achieving accurate relative spacecraft navigation data has already been recognized a decade ago and numerous studies have been conducted to develop adequate data processing strategies and to determine the achievable navigation accuracy (see, e.g., [1,5,7]). While all of the early work

* Corresponding author.
E-mail address: oliver.montenbruck@dlr.de (O. Montenbruck).

1270-9638/02/$ – see front matter
PII: S1270-9638(02)01185-9

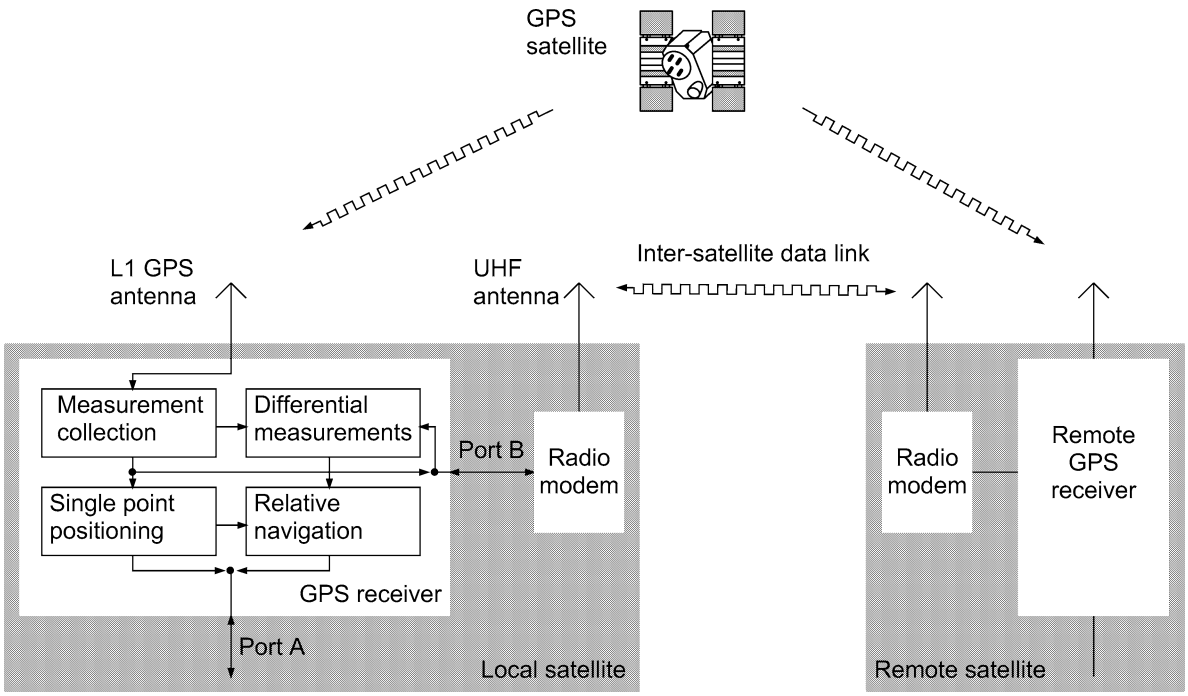

Fig. 1. Conceptual design of a twin GPS receiver system for real-time kinematic relative navigation of two spacecraft.

was based on covariance analyses and numerically simulated GPS measurements, the significance of conducting more realistic hardware-in-the-loop simulations with GPS signal generators and actual space capable GPS receivers has later on been recognized [3,13]. Recently, GPS based approach simulation has successfully been demonstrated in a closed-loop hardware simulation [6].

Traditionally, dedicated navigation processors have been used to dynamically model the absolute and relative motion in a Kalman filter using appropriate scalar or higher-dimensional measurements. External processors provide the required computing power to perform accurate predictions of the spacecraft state vectors under the gravitational and non-gravitational forces but place an additional burden (in terms of, e.g., power consumption, data interfaces, fault tolerance) on the overall navigation system design, which may not be acceptable for future micro-satellite applications. Alternative concepts are therefore desired, which reduce the hardware requirements but still ensure a high navigation accuracy. To this end a kinematic GPS sensor is proposed that directly provides both its own absolute position as well as the relative position of a partner spacecraft without requiring an external navigation processor. A prototype implementation of such a relative navigation sensor has been performed based on the GPS Orion 12-channel L1 receiver. It extends the concept of terrestrial Real-Time-Kinematic GPS navigation using algorithms that are specifically adapted to the conditions of spacecraft navigation with low-cost, low-power single frequency receivers.

The sensor system employs two individual receivers that exchange their raw pseudorange, carrier phase, and Doppler measurements via a dedicated serial data link (Fig. 1). Subsequent to computing its own position and velocity, each receiver processes the differential range and phase after receiving the partner's data set to obtain the relative state vector. The differential processing allows for a high degree of common error cancellation over baselines of typically less than 10 km, which effectively eliminates the impact of broadcast ephemeris errors, ionospheric errors, and GPS satellite clock errors. By smoothing the differential pseudoranges with differential carrier phase measurements, a pronounced reduction of the relative position noise level is achieved. In view of the small relative velocity, time differences of the single-differenced carrier phases provide an excellent approximation of the instantaneous differential range-rate, which also allows a highly accurate determination of the intersatellite velocity vector. Results of hardware-in-the-loop tests using a GPS signal simulator demonstrate the high performance of the novel relative navigation system. Compared to a rigorous dynamical filtering, the overall hardware and software requirements are considerably reduced at a tolerable loss in overall precision. The small size and power consumption of the prototype receiver pair enables their implementation on micro- or nanosatellite platforms with restricted onboard resources, that are commonly considered as candidates for formation flying missions with distributed payloads.

2. Kinematic relative navigation

The relative navigation sensor described in this study assumes a pair of two spaceborne GPS receivers for single frequency C/A code and carrier tracking. The elementary measurements performed by such a GPS receiver may com-

prise pseudorange measurements, carrier phase measurements and Doppler measurements. While pseudorange measurements are obtained from the correlation of the incoming pseudorandom code with an internally generated replica, the phase and Doppler measurements originate in the receiver's phase lock loop (PLL) that tries to maintain a zero difference between the downconverted carrier and a synthesized signal of a digitally controlled oscillator (DCO). If the PLL is properly locked, the integrated carrier phase measurement can be derived from counting integer and fractional DCO cycles. The Doppler measurement in contrast reflects the instantaneous DCO frequency setting and is a direct measure of the incoming frequency and range-rate (at least to the level of the pre-integration interval of, e.g., 1 ms). Alternatively, the range-rate can be determined from the derivative of a polynomial fit of consecutive carrier phase readings. Within the context of the present study, we assume that all three measurement types are supported by two GPS receivers and are available for the absolute and relative navigation. Accuracies of 1 m (pseudorange), 1–10 mm (carrier phase) and 0.1–0.5 m/s (range-rate from phase or Doppler) are achieved by representative single frequency C/A code receivers. By proper combination of all data from two receivers, a highly accurate relative navigation solution can be obtained as discussed in the subsequent sections.

2.1. Observation model and single point positioning

Following [22] the elementary data types pseudorange P, phase $\Phi = \lambda\phi$ and pseudorange-rate D for a single frequency (L1) receiver is modeled as

$$\begin{aligned} P(t) &= \rho(t) + c(\delta t - \delta t_{\mathrm{GPS}}) + I + \varepsilon_P \\ \Phi(t) &= \rho(t) + c(\delta t - \delta t_{\mathrm{GPS}}) + N\lambda - I + \varepsilon_\Phi \\ D(t) &= \dot\rho(t) + c(\delta f - \delta f_{\mathrm{GPS}}) - \dot I + \varepsilon_D \end{aligned} \tag{1}$$

where

$$\rho(t) = \left|\boldsymbol{r}(t) - \boldsymbol{r}_{\mathrm{GPS}}(t-\tau)\right| \tag{2}$$

is the actual range between the receiver at time t and the GPS satellite at signal transmission time,

$$\dot\rho(t) = \boldsymbol{e}^T\left(\dot{\boldsymbol{r}}(t) - \dot{\boldsymbol{r}}_{\mathrm{GPS}}(t-\tau)\right) \tag{3}$$

with

$$\boldsymbol{e}(t) = \frac{\boldsymbol{r}(t) - \boldsymbol{r}_{\mathrm{GPS}}(t-\tau)}{|\boldsymbol{r}(t) - \boldsymbol{r}_{\mathrm{GPS}}(t-\tau)|} \tag{4}$$

is the corresponding range-rate, $N\lambda$ is an unknown bias equal to an integer number of wavelengths, I is the ionospheric path delay, and ε denotes any other error term, including electrical noise, loop errors, and multipath effects, etc., that depend on the receiver characteristics and antenna environment. δt and δf denote the receiver's clock and frequency offset and the index GPS refers to the corresponding quantities of the GPS satellite itself. For completeness we note that the frequency error affecting the Doppler measurements might be different from the derivative of the clock error affecting the pseudorange measurements, if the latter are referred to a computed clock model inside the receiver instead of the free-running reference oscillator.

Making use of the partial derivatives

$$\frac{\partial P}{\partial \boldsymbol{r}} = \frac{\partial \Phi}{\partial \boldsymbol{r}} = \frac{\partial D}{\partial \dot{\boldsymbol{r}}} = \boldsymbol{e} \quad \text{and} \quad \frac{\partial P}{\partial \delta t} = \frac{\partial \Phi}{\partial \delta t} = \frac{\partial D}{\partial \delta f} = 1 \tag{5}$$

a non-linear least-squares adjustment can be used to iteratively obtain the four-dimensional position and clock offset vector $\boldsymbol{x} = (\boldsymbol{r}, c\delta t)^T$ from a set of observed and predicted pseudoranges. Given the linearity of (3), a linear least-squares fit then yields the velocity vector (and frequency offset) from the Doppler (range-rate) measurements (see, e.g., [10,12]).

With a representative dilution of precision of 1 (horizontal plane) to 3 (vertical) the single point positioning results exhibit a typical noise of 1–3 m and 0.1–0.3 m/s, respectively. Superimposed to this are systematic offsets resulting from broadcast ephemeris errors and the neglect of ionospheric refraction that is difficult to model concisely in a real-time space application. Each of these sources may contribute total position errors on the 10 m level (in the absence of Selective Availability effects), but has a negligible contribution to the velocity error budget. Multipath effects may add supplementary position errors depending on the distance and dimension of reflecting surfaces in the vicinity of the receiving antenna.

A further reduction of the position noise level is possible by using carrier phase measurements to smooth the raw pseudoranges in a suitable Kalman filter. Starting from an initial value of $\overline{P}(t_0) = P(t_0)$ at the acquisition of carrier tracking, smoothed pseudoranges at subsequent epochs are obtained as the weighted average

$$\overline{P}(t_i) = P^* + K \cdot \left[P(t_i) - P^*\right] \tag{6}$$

of a predicted value

$$P^* = \overline{P}(t_{i-1}) + \left[\Phi(t_i) - \Phi(t_{i-1})\right] \tag{7}$$

and the residual between the measured pseudorange and P^*. Within the prediction step, the previous filter output is incremented by the range change between epochs as measured by the integrated carrier phase difference. For the real-time implementation, the rigorous computation of the Kalman gain is replaced by the simplified relation

$$K = \begin{cases} 1/i \\ 1/n_{\mathrm{lim}} \end{cases} \quad \text{for} \quad \begin{cases} i < n_{\mathrm{lim}} \\ i \geqslant n_{\mathrm{lim}} \end{cases}, \tag{8}$$

which closely approximates the theoretical values for the applicable ratio of process noise (= carrier phase uncertainty) and measurement noise (= pseudorange uncertainty). At a 10 Hz measurement interval, good results have been obtained for a steady state Kalman gain of $K = 0.004$, which is obtained after $n_{\mathrm{lim}} = 250$ measurements. Slightly different values ($K = 0.02$, $n_{\mathrm{lim}} = 50$) are suggested for a one second filter interval. In view of the code-carrier divergence in

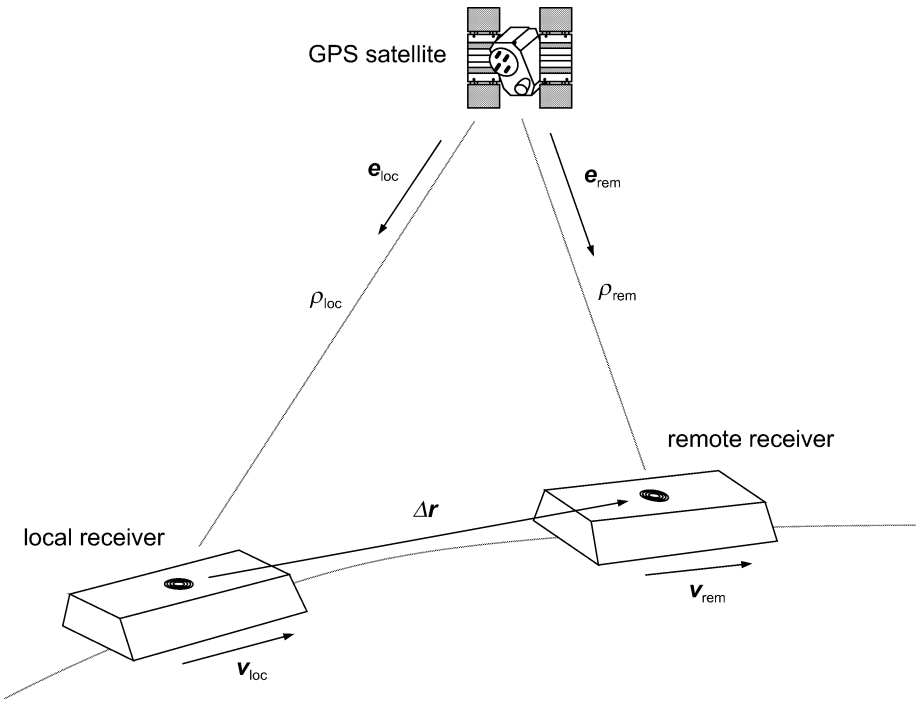

Fig. 2. Modeling of GPS observables for relative navigation of two spacecraft.

dispersive media (as indicated by the opposite signs of I in the observation model (1)) and the possibility of erroneous pseudorange measurements or carrier phase cycle slips, a reset of the filter is required, whenever the difference of predicted and measured pseudorange exceeds a predefined value of, e.g., 5 m.

Concerning a smoothing of the Doppler measurement noise, we note that carrier phase measurements provide highly accurate information on the average range-rate between epochs with a noise level of typically less than 1 cm/s. However, in view of the accelerated motion of both the host vehicle and the GPS satellites, the average range-rate over a one second interval exhibits systematic offsets on the order of 5 m/s from the instantaneous value. At least a second order interpolation over three consecutive carrier phase measurements is therefore required to derive an accurate pseudorange rate measurement for the determination of the absolute spacecraft velocity. The velocity error can thus be reduced to a few cm/s in each axis.

2.2. Differential navigation solution

Based on the locally obtained raw measurements, the receiver obtains its own position $\boldsymbol{r}$ and velocity $\dot{\boldsymbol{r}}$ with representative accuracies of 10 m and 1 m/s, respectively. These values are henceforth assumed as known quantities within the estimation of a relative state vector using additional observations from a remote receiver. Denoting by Δ the (single) difference of quantities referred to the remote receiver (index "rem") minus those of the local receiver (index "loc"), the following observations equations are derived from (1), that relate the differential measurements to the relative state of the two spacecraft (cf. Fig. 2):

$$\begin{aligned}
\Delta P(t) &= \left|\boldsymbol{r}_{\rm loc}(t) + \Delta\boldsymbol{r} - \boldsymbol{r}_{\rm GPS}(t-\tau)\right| \\
&\quad - \left|\boldsymbol{r}_{\rm loc}(t) - \boldsymbol{r}_{\rm GPS}(t-\tau)\right| + c\Delta\delta t + \sqrt{2}\,\varepsilon_P, \\
\Delta\Phi(t) &= \left|\boldsymbol{r}_{\rm loc}(t) + \Delta\boldsymbol{r} - \boldsymbol{r}_{\rm GPS}(t-\tau)\right| \\
&\quad - \left|\boldsymbol{r}_{\rm loc}(t) - \boldsymbol{r}_{\rm GPS}(t-\tau)\right| \\
&\quad + c\Delta\delta t + \Delta N\lambda + \sqrt{2}\,\varepsilon_\Phi, \\
\Delta D(t) &= \boldsymbol{e}_{\rm rem}^T\left(\dot{\boldsymbol{r}}_{\rm rem}(t) - \dot{\boldsymbol{r}}_{\rm GPS}(t-\tau)\right) \\
&\quad - \boldsymbol{e}_{\rm loc}^T\left(\dot{\boldsymbol{r}}_{\rm loc}(t) - \dot{\boldsymbol{r}}_{\rm GPS}(t-\tau)\right) + c\Delta\delta f + \sqrt{2}\,\varepsilon_D \\
&= \boldsymbol{e}_{\rm rem}^T\Delta\dot{\boldsymbol{r}}(t) + \Delta\boldsymbol{e}^T\left(\dot{\boldsymbol{r}}_{\rm loc}(t) - \dot{\boldsymbol{r}}_{\rm GPS}(t-\tau)\right) \\
&\quad + c\Delta\delta f + \sqrt{2}\,\varepsilon_D. \qquad (9)
\end{aligned}$$

Here, the signal light time has been set equal for both receivers, which is accurate to the 100 ns level and introduces modeling errors of less than 0.4 mm for relative separations below 30 km. Likewise the differential ionospheric path delay has been neglected for the concerned baselines. No other simplifications are involved in the above equations, however. In particular a Taylor series expansion of the distance between receiver and GPS satellite is avoided to ensure proper applicability of the results for a receiver separation of 1 km and higher.

As in the absolute positioning, the non-linear observation equation for the differential pseudorange requires an iterated least-squares solution to obtain the differential position and clock vector $\Delta\boldsymbol{x} = (\Delta\boldsymbol{r}, c\Delta\delta t)^T$. For a set of n differential

pseudorange observations (smoothed or unsmoothed) the design matrix is given by

$$\boldsymbol{A} = \begin{pmatrix} \dfrac{\partial \Delta P_1}{\partial \Delta \boldsymbol{x}} \\ \vdots \\ \dfrac{\partial \Delta P_n}{\partial \Delta \boldsymbol{x}} \end{pmatrix} = \begin{pmatrix} \boldsymbol{e}_{1,\mathrm{rem}}^T & 1 \\ \vdots & \vdots \\ \boldsymbol{e}_{n,\mathrm{rem}}^T & 1 \end{pmatrix}, \tag{10}$$

where the unit vectors

$$\begin{aligned} \boldsymbol{e}_{\mathrm{rem}} &= \frac{\partial}{\partial \Delta \boldsymbol{r}} \big| \boldsymbol{r}_{\mathrm{loc}}(t) + \Delta \boldsymbol{r} - \boldsymbol{r}_{\mathrm{GPS}}(t-\tau) \big| \\ &= \frac{\partial}{\partial \boldsymbol{r}_{\mathrm{rem}}} \big| \boldsymbol{r}_{\mathrm{rem}}(t) - \boldsymbol{r}_{\mathrm{GPS}}(t-\tau) \big| \end{aligned} \tag{11}$$

describe the partial derivatives of the slant range from the remote spacecraft to the GPS satellite at the respective measurement epochs.

Denoting by $\boldsymbol{b}$ the vector of observed minus modeled differential pseudoranges (cf. (9)), an initial value of $\Delta \boldsymbol{x}$ is improved from the solution of the corresponding normal equations:

$$\Delta \boldsymbol{x}^{\mathrm{upd}} = \Delta \boldsymbol{x} + \big(\boldsymbol{A}^T \boldsymbol{A}\big)^{-1} \big(\boldsymbol{A}^T \boldsymbol{b}\big). \tag{12}$$

Starting from an a priori value of $\Delta \boldsymbol{x} = (\boldsymbol{0}, 0)$, the iteration typically converges within two steps. Based on the resulting position estimate for the remote spacecraft, the line-of-sight vector differences can then be obtained, which enter the differential Doppler measurement equations. From these, the relative velocity and differential clock rate $\Delta \dot{\boldsymbol{x}} = (\Delta \dot{\boldsymbol{r}}, c\Delta\delta f)^T$ of both spacecraft is finally obtained using a linear least-squares estimation. Since the range rate equation in (9) is linear in $\Delta \dot{\boldsymbol{r}}$ and $\Delta \delta f$, no iteration is required and the desired parameters can directly be computed from the vector $\dot{\boldsymbol{b}}$ of observed minus modeled differential range rates

$$\Delta \dot{\boldsymbol{x}} = \big(\boldsymbol{A}^T \boldsymbol{A}\big)^{-1} \big(\boldsymbol{A}^T \dot{\boldsymbol{b}}\big) \tag{13}$$

with modeled values computed for $\Delta \dot{\boldsymbol{x}} = (\boldsymbol{0}, 0)$.

Assuming uncorrelated measurement errors, the single difference measurements exhibit a noise level that is $\sqrt{2}$ times as large as that of the undifferenced data. Using only pseudorange and Doppler measurements, the resulting relative navigation solution therefore exhibits an increased standard deviation of roughly 2–5 m and 0.2–0.5 m/s (r.m.s.). However, the solution is essentially bias free due to the (at least partial) cancellation of broadcast ephemeris errors and ionospheric errors.

For an effective reduction of the noise level, the carrier phase smoothing concept described in Eqs. (6)–(7) is likewise applied to the single-differenced data types. In contrast to the individual receiver measurements, the differenced pseudorange and carrier phase are essentially free of ionospheric effects. As such, the smoothing process for the differential measurements is not affected by the code-carrier divergence and requires only very few resets even during extended measurement arcs.

The comparatively small relative speed (< 10 m/s for a 10 km separation) and differential acceleration of two space vehicles in controlled proximity, furthermore, allows an effective replacement of differential Doppler measurements by time and receiver differenced carrier phases. To this end a 2nd order interpolating polynomial is constructed from three consecutive differential carrier phase measurements $\Delta\Phi_{i-2}$, $\Delta\Phi_{i-1}$, and $\Delta\Phi_i$ obtained at time steps $t_i - 2dt$, $t_i - dt$, and t_i. Differentiation of this polynomial then results in the following difference quotient approximation for the time derivative of the differential carrier phase at the latest measurement epoch:

$$\begin{aligned} \Delta\dot{\Phi}(t_i) &\approx \frac{1}{2dt}\big(3(\Delta\Phi_i - \Delta\Phi_{i-1}) - (\Delta\Phi_{i-1} - \Delta\Phi_{i-2})\big) \\ &= \frac{3\Delta\Phi_i - 4\Delta\Phi_{i-1} + \Delta\Phi_{i-2}}{2dt}. \end{aligned} \tag{14}$$

It may be used as a replacement for the Doppler derived differential range rate $\Delta D(t)$ in the observation model (9). The above linear combination of multiple phase measurements yields a resulting noise of

$$\varepsilon_{\Delta\dot{\Phi}} = \frac{\sqrt{3^2+4^2+1^2}}{2}\frac{\sqrt{2}\varepsilon_\Phi}{dt} = \sqrt{13}\frac{\varepsilon_\Phi}{dt}, \tag{15}$$

which amounts to roughly 4 mm/s for a representative measurement interval of $dt = 1$ s and a 1 mm carrier phase noise and is thus notably smaller than the differential Doppler noise. In view of moderate velocity changes during the averaging interval, the difference quotient approximation yields only minor errors in the measured relative range-rate and is far outweighed by the pronounced noise reduction. In total, relative velocities can thus be determined with a representative accuracy of better than 1 cm/s as shown by corresponding hardware-in-the-loop simulations.

2.3. Local orbital reference frame

In accordance with [2] the absolute navigation solution is traditionally performed in an Earth-fixed coordinate system (WGS84), which is therefore also used in the relative positioning. For an intuitive interpretation of the relative location of two spacecraft orbiting the Earth in close proximity it is more suitable, however, to express the differential state vector in a reference frame aligned with the local radial (R), along-track (tangential, T) and cross-track (normal, N) directions. The corresponding unit vectors of this reference frame are defined by

$$\boldsymbol{e}_{\mathrm{R}} = \frac{\boldsymbol{r}}{|\boldsymbol{r}|}, \qquad \boldsymbol{e}_{\mathrm{N}} = \frac{\boldsymbol{r}\times\boldsymbol{v}}{|\boldsymbol{r}\times\boldsymbol{v}|}, \qquad \boldsymbol{e}_{\mathrm{T}} = \boldsymbol{e}_{\mathrm{N}} \times \boldsymbol{e}_{\mathrm{R}}, \tag{16}$$

where all quantities refer to the local receiver and the inertial velocity

$$\boldsymbol{v} = \dot{\boldsymbol{r}} + \boldsymbol{\omega}_\oplus \times \boldsymbol{r} \tag{17}$$

is obtained by correcting the derivative of the WGS84 position for the angular velocity $\boldsymbol{\omega}_\oplus$ of the Earth's rotation.

While the relative RTN position vector is obtained by direct projection on the above base vectors, the corresponding relative velocity transformation needs to account for the inertial rotation of the RTN triad about the N axis:

$$\begin{aligned}\Delta\boldsymbol{r}_{\mathrm{RTN}} &= (\boldsymbol{e}_{\mathrm{R}}, \boldsymbol{e}_{\mathrm{T}}, \boldsymbol{e}_{\mathrm{N}})^T \Delta\boldsymbol{r},\\ \Delta\dot{\boldsymbol{r}}_{\mathrm{RTN}} &= (\boldsymbol{e}_{\mathrm{R}}, \boldsymbol{e}_{\mathrm{T}}, \boldsymbol{e}_{\mathrm{N}})^T (\Delta\dot{\boldsymbol{r}} + \boldsymbol{\omega}_{\oplus} \times \Delta\boldsymbol{r})\\ &\quad - (0, 0, \omega_{\mathrm{N}})^T \times \Delta\boldsymbol{r}_{\mathrm{RTN}}. \end{aligned} \tag{18}$$

The corresponding instantaneous rotation rate

$$\omega_{\mathrm{N}} = \left(\boldsymbol{e}_{\mathrm{T}}^T \boldsymbol{v}\right)/|\boldsymbol{r}| \tag{19}$$

is given by the ratio of the along-track velocity and the distance from the center of the Earth. In the absence of thrust arcs, the evolution of the RTN relative state is approximately described by the well-known Clohessy–Wiltshire (or Hill's) equations [4]. This is useful for a visualization of the relative motion, a rapid forecast (e.g., in rendezvous-type proximity operations) and for an optional dynamical filtering of the purely kinematic relative navigation solution. Furthermore, the decoupling of the relative motion equations in the RTN frame (cf. [26]) allows a straightforward planning and analysis of orbital maneuvers for the maintenance or acquisition of a desired relative configuration.

3. GPS receiver description

3.1. Prototype design

The GPS Orion receiver (cf. Fig. 3) used in the present study represents a prototype design of a terrestrial GPS receiver built around the Mitel (now Zarlink) GP2000 chipset [15]. It comprises a GP2015 R/F front end and DW9255 saw filter, a GP2021 correlator as well as an ARM60B 32-bit microprocessor. The receiver provides C/A code tracking on 12 channels at the L1 frequency and operates with an active antenna having a total gain of roughly 28 dB. The main receiver board measures about 5 cm × 10 cm and is complemented by an equally sized interface in the prototype receiver design. The interface board carries a switching regulator, line drivers for the two serial I/O ports as well as a rechargeable NiCd battery to maintain the real-time clock and non-volatile memory inside the receiver while disconnected from the main power supply. In space applications, the standard interface board is subject to replacement with tailor made solutions in accord with the spacecraft power and communications architecture. The power consumption of the receiver itself amounts to 2 W at 5 V supply voltage, resulting in a total of 2.4 W when accounting for the losses of the switching regulator.

The receiver software is stored in two EPROMs with a capacity of 256 kB and loaded into a twice as large RAM memory at boot time. Typical code sizes of software versions in current use range from 160–200 kB. A task switching operating system allows a quasi-concurrent execution of high- and low-priority activities and flexible activation cycles for individual receiver tasks. To support user specific software adaptations for the GPS Orion receiver, the GPS Architect [14] development kit has (up to recently) been made available by Mitel Semiconductors. The Architect receiver is essentially hardware compatible to the Orion receiver but allows software uploads and debugging via a supplementary serial interface port. On the other hand, the Architect does not support a battery buffered non-volatile memory and real-time clock. The GPS Architect supercedes the GPS Builder-2 development kit for the GPS2015/2021 chipset provided previously by GEC-Plessey [9].

3.2. Space adaptation

For use on low Earth satellites and other space applications numerous modifications and enhancements have been made to the original firmware of the Orion receiver [17], which was implicitly based on the assumption of a low speed vehicle. This resulted in the neglect of the user velocity in the Doppler prediction, the neglect of the topocentric frame rota-

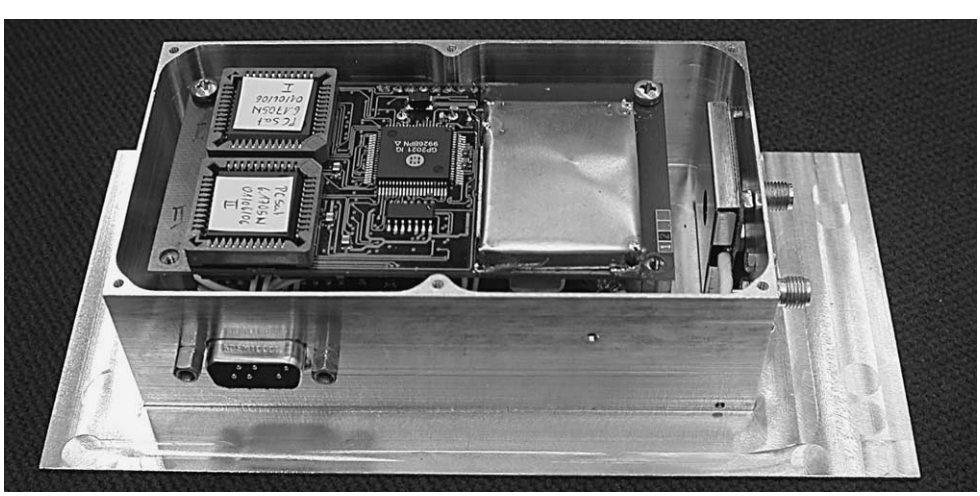

Fig. 3. Orion GPS receiver (PCsat flight unit).

tion in the spherical formulation of the single point positioning, the neglect of acceleration in the subsequent filtering of the navigation solution and the ignoring of a 1 ms time tagging error of the raw measurements [20]. Aside from these fixes, multiple extensions have been made to the command and telemetry interface of the receiver to allow convenient and flexible operation of the receiver via a remote data link and to adapt the receiver output to the available downlink capacity.

To ensure a robust tracking and rapid signal acquisition under the conditions of a high-dynamics space vehicle an open-loop Doppler and visibility prediction algorithm [16] has been added to the receiver code. Depending on the vehicle characteristics, either a polynomial approximation of the trajectory (sounding rockets, reentry vehicles) or an analytical orbit model (LEO satellites) is employed in this position-velocity aiding. Making use the SGP4 orbit theory [8], sufficiently accurate predictions can be obtained from publically available NORAD twoline element sets that are uploaded to the receiver about once per week. Practical tests of the aiding concept in a signal-simulator environment as well as flight data from the PCsat mission have demonstrated times-to-first-fix of 20–60 s under hot start conditions [19,21].

While the original Orion firmware collects measurements at equidistant time steps beginning at boot time, an active alignment of measurements epochs and navigation solutions to the integer second of GPS time has been implemented in the revised version. The accuracy of the alignment is determined by the limited resolution of the tic length settings supported by the GP2021 correlator and the overall C/A code single point positioning accuracy. In the absence of Selective Availability the alignment is generally accurate to better than 200 ns. Supplementary to the internal alignment of measurements and navigation, the modified Orion receiver generates a hardware signal (pulse-per-second) of 1 ms duration at the occurrence of each integer second that can be used for onboard clock synchronization purposes.

To improve the overall navigation performance of the Orion receiver, integrated carrier phase measurements have been made available using appropriate readouts of the digitally controlled oscillators (DCO). In parallel, the 2nd order frequency lock loop (FLL) of the GPS Architect was supplemented by a 3rd-order, FLL assisted phase lock loop (PLL) (cf. [25,27]), which ensures an optimum signal acquisition performance and accurate tracking of the carrier phase under high dynamics. A PLL of 3rd order does not exhibit acceleration dependent errors, which is well illustrated by the signal simulator tests (cf. Section 4.2). The carrier phase measurements are used to compute smoothed pseudoranges based on a simple filter as described in Section 2.1. The actual smoothing is carried out inside the measurement task as part of the measurement collection process at a 10 Hz update rate. The smoothed pseudoranges are subsequently used to compute the single point position solution and clock offset correction which thus exhibit a notably smaller noise level than in the unsmoothed case.

While the above adaptation of the receiver software ensures proper tracking performance under the dynamical signal conditions of a space mission, no special efforts have so far been made to adapt the Orion hardware to the associated environmental conditions. However, it has been demonstrated previously (cf. [23]) that the components of the employed GP2000 chipset are sufficiently radiation proof (> 10 krad) to allow a meaningful use in low Earth orbits (500–800 km altitude) without major modifications. Considering a shielding of, e.g., 3 g/cm^2 aluminum as provided by representative bus structures, a lifetime of several years may be expected before the total radiation dose results in a significant degradation of the components. As a limited protection against latch-up effects a supplementary electronic fuse is, however, recommended to limit the total current consumption. The unmodified Orion receiver is presently undergoing flight tests onboard the PCsat microsatellite [19] and the University of Surrey's SGR-05 receiver sharing most of the Orion's design aspects has successfully been operated on the SNAP-1 mission [24]. Despite the lack of a full space qualification, the Orion receiver can therefore be considered as a suitable baseline for a formation flying technology demonstration mission.

3.3. Relative navigation

The Orion receiver provides two serial ports, which can be freely programmed to perform any desired input/output function. Typically the primary port (A) is connected to the spacecraft bus (or a monitoring and control PC) and used to configure relevant receiver parameters and to collect the generated output messages. For the relative navigation application, we employ the auxiliary data port (B) as a dedicated interface for the exchange of raw measurements and between a pair of receivers remotely connected by a serial radio link (Fig. 1). In the present implementation unsmoothed pseudoranges, carrier phase measurements and Doppler data are output in a single ASCII data message comprising a total of 0.5 kB. For test purposes, a separate output message of 0.1 kB size provides the receiver's internal navigation solution. At a 19.6 kB data rate a total of roughly 2000 characters can be transmitted per second, thus requiring about 0.3 s for the data exchange between receivers.

For minimum latency, the tasking inside the receiver has been modified in such a way as to start the data output immediately after completion of the navigation solution. The latter step is generally finished within 0.1–0.3 s after obtaining the raw measurements from the corresponding low level correlator readings. The synchronization of the measurement collection (and the navigation solution epoch) to integer GPS seconds implies that both the remote and local receiver obtain their measurements at the same time within a limit of less than a microsecond. Since both receivers apply a

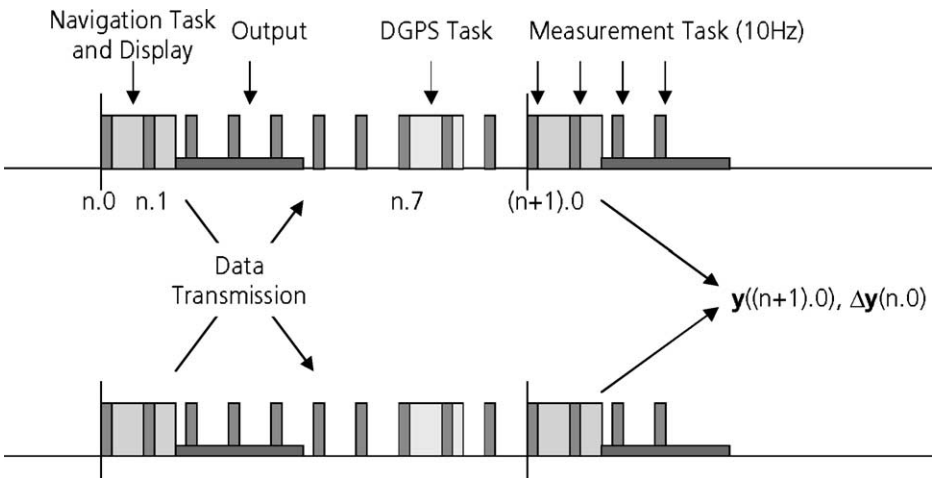

Fig. 4. Scheduling of measurement collection (10 Hz), absolute and relative navigation as well as data output inside the modified Orion receiver.

coherent task activation scheme, corresponding output messages are also generated at near identical times, even though different CPU loads (caused by, e.g., a varying number of tracked channels) may result in a scatter of about 0.2 s.

Based on the above timing considerations, a new relative navigation task has been introduced, which is activated at 0.7 s after the integer second (Fig. 4). It scans the auxiliary data port for new messages received since its last activation, reads and extracts any raw measurements of the remote receiver and uses these together with its own raw measurement to compute a differential navigation solution in accord with the algorithms presented in Section 2. The selected task activation time ensures that the remote data transfer has been completed under normal operations workload, while leaving sufficient time for the required computations. After completion of the relative navigation task the resulting differential position and velocity estimate is stored for output by the display function which is activated right at the end of the next (absolute) navigation task. As a consequence of the employed processing scheme, the relative navigation solution always has a latency of one second with respect to the absolute navigation information. This is mainly driven by the assumed data link and CPU performance and can be reduced when using more powerful hardware components. In general, however, the quoted figures are considered tolerable, since the relative state of two spacecraft varies notably less than their absolute position and velocity.

4. Hardware-in-the-loop testing

4.1. Test configuration

For a qualification of the relative navigation system, intensive hardware-in-the-loop simulations were conducted using a Spirent STR4760 GPS signal simulator capable of simulating L1 signals for 2 vehicles on up to 16 channels each (Fig. 5). In all cases the receivers were directly connected to the simulator R/F output via cables and a 28 dB low noise amplifier, i.e., the simulations did not involve a hardware antenna. However, this is considered an acceptable restriction compared to the detrimental effects that wall reflections and a superposition of two signal sources would have created in an open transmission of the simulated R/F signals inside the laboratory environment.

Visible satellites and signal levels were simulated based on the assumption of a near hemispherical, zenith looking antenna with a sharp sensitivity drop below 5° elevation. The simulator's internal amplification was adjusted to obtain peak signal-to-noise readings of 19 dB (as indicated by the Orion receiver) that matched those of outdoor tests with representative active antennas.

4.2. Single receiver tracking performance

The native measurement accuracy of the Orion receiver in a spaceborne application was analyzed for a polar low Earth orbit of 87° inclination and 450 km altitude, which involves a widely varying satellite visibility and notable signal dynamics. No ionospheric delays (or ephemeris errors) were considered in the initial simulation setup, but separate tests were conducted to show the overall impact of these effects on the resulting navigation accuracy. For all tests, the Orion receiver was configured to allow tracking of GPS satellites above zero degrees elevation but to include only satellites above 10° in the navigation solution. The different elevation masks effectively prevent occasional pseudorange measurements of low quality near acquisition or measurement dropouts from affecting the overall navigation accuracy.

After collecting the raw measurements over a two hour data arc, modeled pseudoranges and range rates were computed based on the simulated spacecraft trajectory and the known GPS constellation almanac. These were subsequently subtracted from the measurements to remove the varying geometry between the receiver and the GPS satellites from the data (cf. Fig. 6). The result is essentially the sum of receiver clock errors ($\delta t, \delta f$), as well as measurement noise

Fig. 5. Formation flying simulation setup showing the STR4760 signal simulator, two Orion GPS receivers with external preamplifiers (VAS Aerospace) and a host PC attached to one receiver for configuration and data recording. The data exchange between the auxiliary data ports is performed via two UHF radio modems (ADCON).

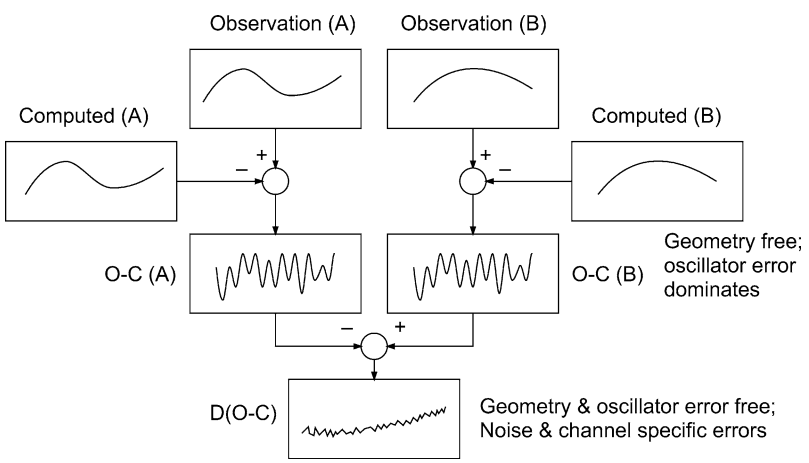

Fig. 6. Processing scheme for the accuracy assessment of single receiver raw measurements obtained in signal simulator tests.

and tracking loop related errors (ε_i). To further eliminate the dominating clock terms, differences of two channels were subsequently formed. Ideally, this results in a zero mean white noise sequence with a variance equal to the sum of the noise variance of the individual channels. For two channels with similar signal-to-noise (SNR) ratios, the noise errors are expected to be of equal size and the r.m.s. noise of the inter-channel difference is just $\sqrt{2}$ times as large as that of the undifferenced measurements.

Sample results obtained in the above manner are shown in Fig. 7 for the difference of two satellites having favorable signal levels and a common visibility interval of roughly 15 min. The derived noise of the undifferenced measurements amounts to typically 0.9 m (pseudorange), 0.8 mm (carrier phase), and 0.08 m/s (Doppler/range-rate), respectively. Slightly higher noise figures have been obtained for carrier phase and Doppler measurements at low SNR ratios, whereas the pseudorange measurements have an essentially uniform quality over the applicable range of signal conditions. Neither of the data types exhibits signs of systematic errors, thus confirming the proper function of the employed 3rd order phase lock loop, which is insensitive to line-of-sight accelerations.

Aside from the raw measurement accuracy, the real-time navigation performance achieved with the Orion receiver depends on the size of broadcast ephemeris errors and uncor-

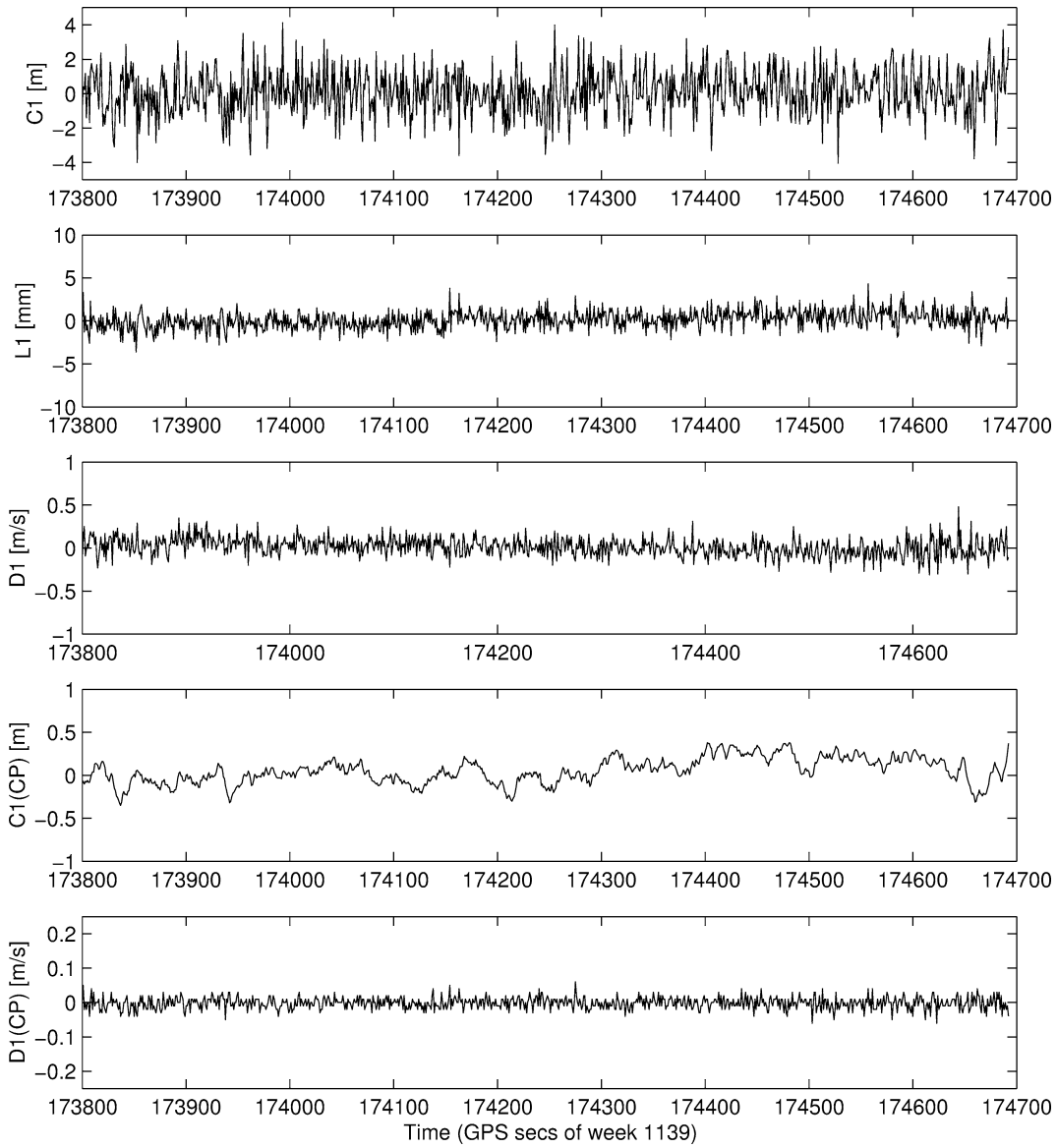

Fig. 7. Interchannel differences of pseudorange (C1), carrier phase (L1) and Doppler (D1) measurements collected by the Orion GPS receiver in a hardware-in-the-loop test relative to simulated values (cf. Fig. 6). The noise of the undifferenced measurements amounts to 0.9 m, 0.8 mm, and 0.08 m/s, respectively. Carrier phase smoothed pseudoranges (C1(CP)) exhibit an rms error of 0.1–0.2 m and carrier based range rates are typically accurate to 0.02 m/s.

rected ionospheric path delays as well as multipath effects. Typically, only the position solution is affected by these error sources in view of the pronounced Doppler measurement noise that dominates the overall uncertainty of the estimated velocity vector. In accord with a representative dilution-of-precision (DOP) of 1 for the horizontal plane and 3 for the vertical direction, individual single point solutions from pseudorange and carrier measurements exhibit a typical data noise of 1 m to 3 m and 0.1 m/s to 0.3 m/s in the absence of other errors. Using carrier phase smoothed pseudorange, the r.m.s. noise can further be reduced to 0.15–0.5 m, even though peak errors (near resets of the smoothing filter) may still be as large as 1–2 m. In the presence of broadcast ephemeris errors, the resulting position errors increase in direct proportion to the assumed ephemeris errors and amount to roughly 5–10 m for an S/A free GPS constellation. While the position solution is still smooth over time scales of several minutes due to the carrier phase smoothing, sudden jumps are observed whenever the set of tracked GPS satellites changes. These jumps may be several meters in size depending on the ephemeris errors of the particular GPS satellite acquired or lost at that instant.

Ionospheric path delays, which are not accounted inside the Orion receiver s/w for an orbiting spacecraft, result in a moderately increased scatter of the resulting position solution in all axes as well as a systematic radial bias that is somewhat less than the vertical path delay. A general discussion of ionospheric errors for spaceborne single frequency GPS receivers is given in [18], which also addresses possible compensation schemes. The performance degradation of

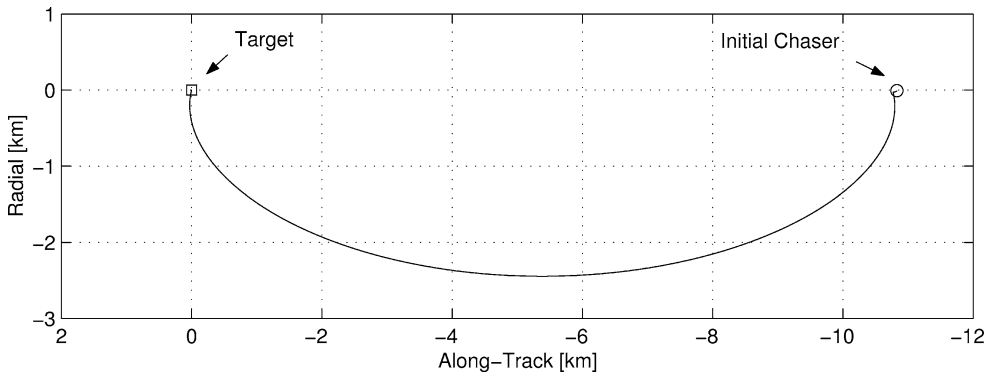

Fig. 8. Relative motion of the chaser and target vehicle within the common orbital plane during the simulated rendezvous scenario. A two-impulse elliptical transfer orbit is used to remove the initial along-track separation within a specified flight time of 60 min.

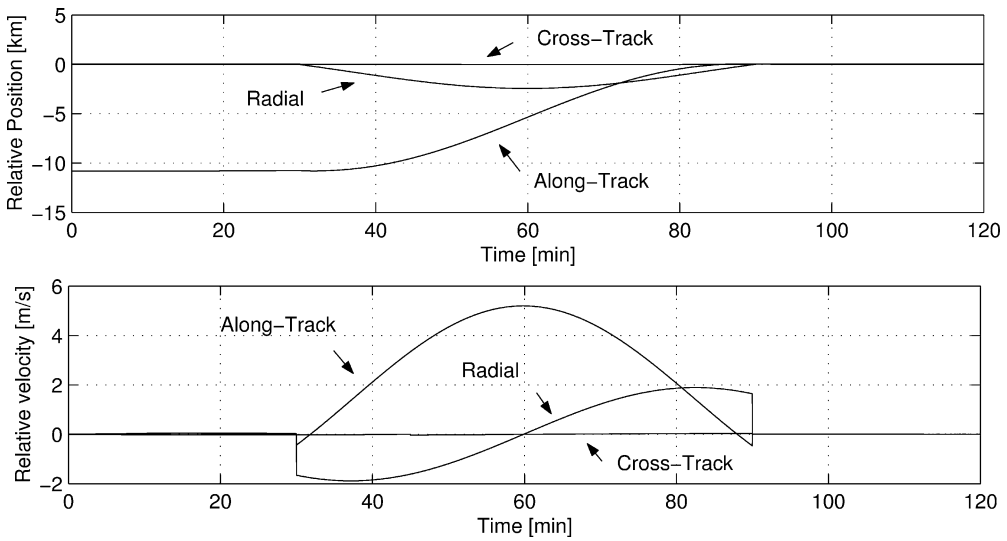

Fig. 9. Relative position and velocity of the chaser vehicle with respect to the target. The configuration is stationary for 30 min before and after the orbital transfer.

the Orion position solution observed in the signal simulator tests is in general agreement with the experience gathered in that study from flight data of the Champ dual frequency GPS receiver. Overall, however, the comparison suffers from the simplifying ionospheric refraction model employed in the available GPS signal simulator, which inhibits a more detailed and realistic assessment of ionospheric error contributions to the absolute navigation solution.

4.3. Relative navigation performance

The kinematic relative navigation performance was evaluated in a typical rendezvous trajectory with two impulsive burns. The target trajectory is a near-circular orbit (0.001 eccentricity) in a Space Shuttle altitude of 300 km and inclination of 51.6 degrees. The chaser satellite is initially in the same orbit about 10 km behind the target on the along-track direction. Both satellites are orbiting passively for the first 30 minutes maintaining roughly the same separation distance. At the simulation time $t = 30$ min, the transfer burn is applied to the chaser to intercept the target within an hour. The impulsive velocity vector was obtained by solving the Lambert targeting problem, and the resulting chaser trajectory is a non-Hohmann transfer orbit (Fig. 8) as may be recognized from the predominantly radial burn direction. At the end of the transfer sequence, a stop burn is applied at $t = 90$ min to align the chaser velocity vector with the target velocity vector. After the stop burn, the proximity phase with a 2–5 m baseline length lasts another 30 min. Fig. 9 shows the relative position and velocity of the chaser with respect to the target during the entire simulation period of two hours.

Motion data based on a realistic trajectory model and the required maneuvers for both vehicles were generated on an external control computer and used to steer the Spirent STR4760 signal simulator via the real-time interface. A constant total electron content (TEC) of 2×10^{17} m^{-2} was selected for the modeling of ionospheric path delays. In addition, broadcast ephemeris errors of several meters were intentionally added to each GPS satellite but no intentional clock dithering was applied in the simulation in accord with the present policy for use of Selective Availability (S/A). The GPS satellite dependent range errors are expected to affect

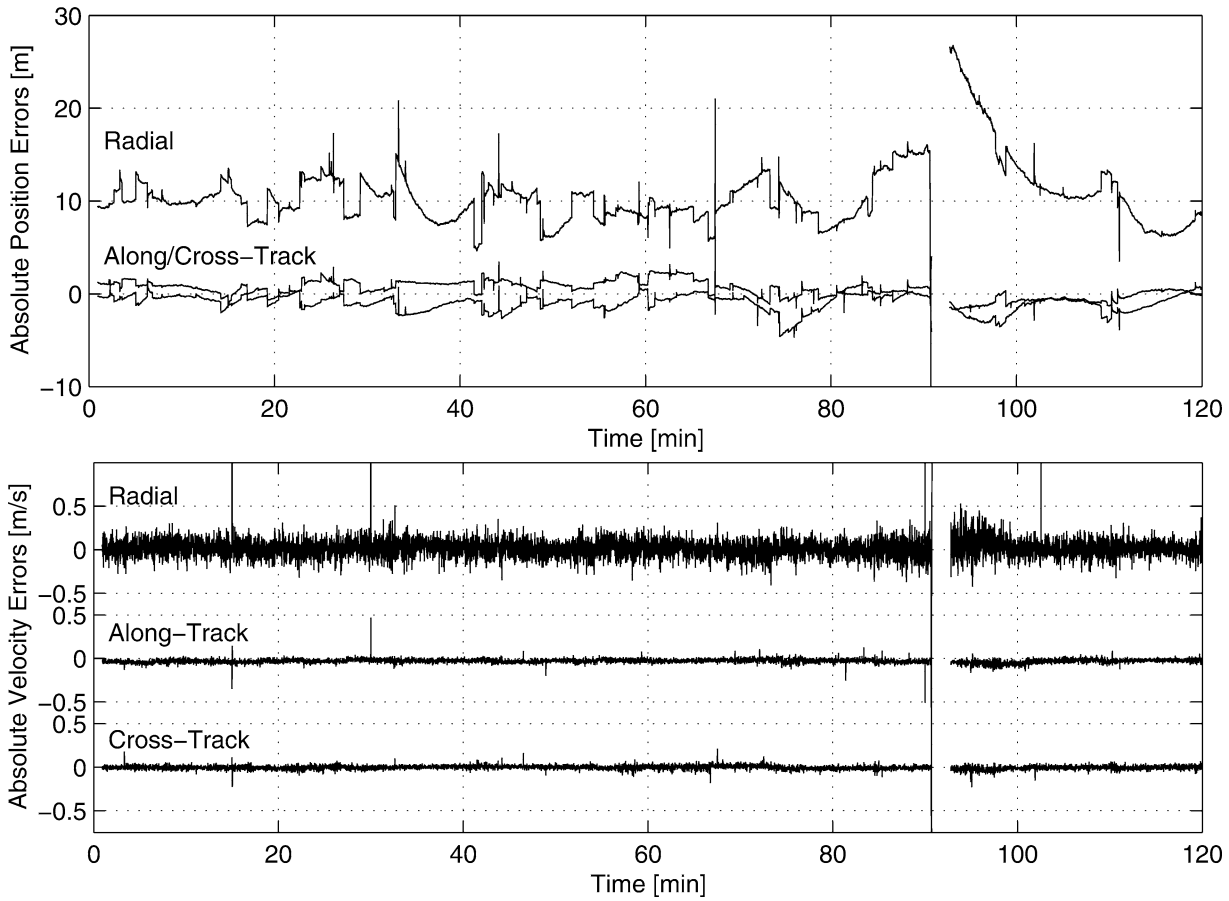

Fig. 10. Errors of the GPS based single point solutions for position and velocity using carrier phase smoothed L1 C/A code pseudoranges and L1 Doppler measurements in the presence of broadcast ephemeris errors and uncorrected ionospheric path delays.

only the absolute navigation accuracy but to be properly removed in the relative navigation solutions. Multipath effects, which are highly dependent on the actual antenna system and spacecraft design have not been considered in the simulation due to the lack of suitable models. Since the multipath environment cannot be assumed to be identical for both spacecraft, these errors do not cancel out when forming differenced observations and the navigation accuracy will generally degrade compared to the present simulations. Range multipath errors are expected to be most pronounced in the vicinity of large structures with reflecting surfaces like a space station or manned vehicle. Phase multipath in contrast would also be observed on small satellites but be limited to the size of a wavelength.

A sample plot of the absolute navigation solution performance obtained from the above simulation settings is shown in Fig. 10. Stepwise changes of the position errors are related to the varying contribution of broadcast ephemeris errors as new GPS satellites are acquired or previously tracked satellites are lost. The short time noise level of the position error, however, is reduced to 0.1–0.5 m by using carrier smoothed pseudorange measurements and spike errors of several meters are only observed at occasional filter resets. The ionospheric range delay, which remains uncorrected in the Orion receivers, induces an average radial position offset of about 10 m. Changes of the ionospheric refraction related to rapidly varying elevation angles of the tracked GPS satellites are, furthermore, apparent from a notable bending of the position error curve over time scales of 5 to 10 min. The absolute velocity errors shown in Fig. 10 are dominated by the range-rate measurement noise rather than the ionospheric and broadcast ephemeris errors and exhibit a typical standard deviations of 0.06–0.10 m/s in the radial direction and 0.02–0.04 m/s in the along- and cross-track directions.

Near $t = 90$ min, a gradual deterioration and temporary loss of the navigation solution may be observed, which results from an unfavorable observation geometry (high PDOP) and an insufficient number of GPS satellites above the specified 10° elevation mask during the respective time interval. Even though continuous tracking could have been ensured by a 5° limit, an occasional loss of 3D single point navigation fixes is considered a common problem in LEO satellite applications and no attempt has been made to hide this problem in the present simulation.

The high level of common error cancellation obtained in the relative navigation solution at distances of 0–10 km is obvious from Fig. 11, which shows the errors of the RTN relative coordinates of the target and chaser vehicle. Other

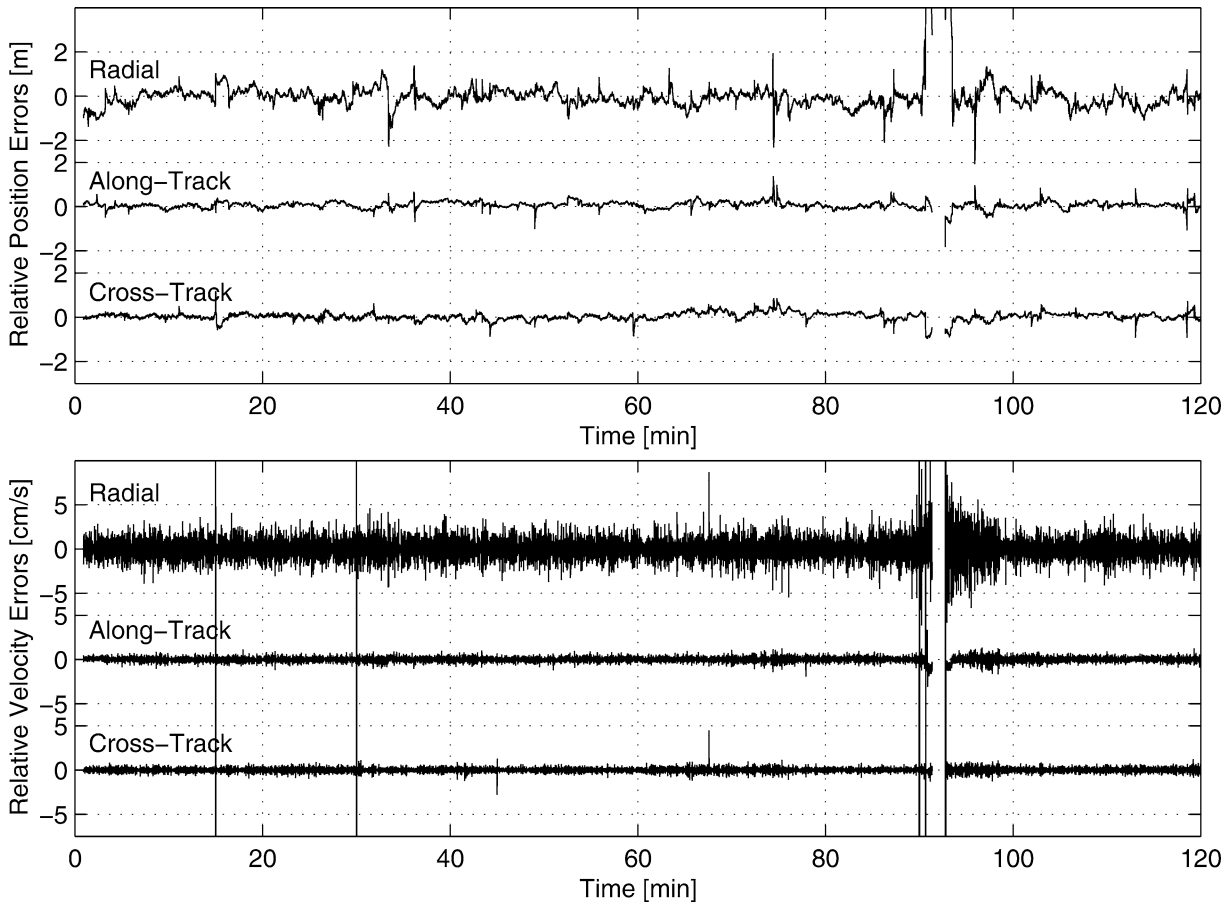

Fig. 11. Errors of the kinematic relative navigation solution in the local orbital frame using carrier phase smoothed differential pseudoranges and time differenced differential carrier phase measurements.

than the absolute position, the relative position solution is essentially unaffected by both the broadcast ephemeris errors and the ionospheric refraction. An r.m.s. accuracy of 0.15 m is achieved in the along-track direction, while the accuracy of the radial component is slightly worse (0.3–0.5 m) in view of the less favorable vertical dilution of precision. For completeness we note that the use of an RTN frame for the relative vehicle coordinates requires accurate knowledge of the absolute velocity vector to properly determine the along-track and cross-track direction. To ensure a 0.1 m relative position accuracy at a 10 km along-track separation, the velocity vector must be known to 10 ppm or 7 cm/s. Early tests with less accurate, Doppler based range-rate measurements have indeed shown an increased noise level in the cross-track relative position during the initial phase of the rendezvous scenario.

The relative velocity vector of the target and chaser vehicle exhibits an r.m.s. noise of 2–10 mm/s (cf. Fig. 11), which complies well with a 2.5 mm/s noise of the carrier based range rate measurements at the 1 s sampling interval and representative horizontal and vertical dilution of precision values.

Strictly speaking, all figures quoted above refer to the accuracy with which the relative position and velocity of the GPS antennas on the remote and local spacecraft can be determined. To fully utilize the achievable sensor precision for navigation purposes or science data analysis it may be required to account for a center-of-mass correction using spacecraft attitude information. For spacecraft aligned with the local orbital frame (e.g., remote sensing satellites) this correction represents a (near-)constant offset in the RTN relative coordinates that can readily be configured within the attitude and orbit control system (AOCS). Otherwise, supplementary attitude information may be exchanged via the available radio link to obtain instantaneous center-of-mass corrections.

5. Summary and conclusions

The concept of a simple, yet accurate, relative navigation system for space applications has been presented. It is based on a pair of single frequency GPS receivers exchanging their raw measurements via a radio link to compute the relative position and velocity in addition to their absolute state vector. A purely kinematic processing is applied that makes no assumptions on the dynamics of motion and can readily be accommodated inside the receivers. Despite

these simplifications, a remarkable performance is achieved in view of significant common error cancellation and a processing scheme that makes extensive use of highly accurate carrier phase measurements. Using a prototype implementation hosted on two Mitel Orion receivers, r.m.s. errors in the relative state vector components of typically 0.5 m and 1 cm/s have been demonstrated in hardware-in-the-loop simulations. This should well serve the needs of approach navigation in rendezvous and docking applications down to distances of about 10 m, where optical (see, e.g., [11]) or other near-field sensors are expected to take over at the latest. If necessary, the system can readily be extended to support pseudolite augmentation systems [28] if signal blockage poses a problem in the vicinity of large space structures. Even though further accuracy improvements could be obtained by using geodetic quality dual frequency receivers providing more accurate raw measurements and allowing an on-the-fly carrier phase ambiguity resolution, the presented system provides a favorable trade-off between overall effort, system cost and achieved performance. This makes the system attractive for use on small formation flying satellites with distributed payloads that are considered a key technology for more effective space missions.

Due to the purely kinematic nature of the relative navigation solution, the proposed system is essentially insensitive to velocity changes performed on either of the vehicles and can thus provide reliable state estimates across thrust arcs or impulse maneuvers without a priori information on such events. Despite these advantages, it is evident that a kinematic navigation solution bears the risk of drop-outs due to insufficient GPS visibility conditions. This is well illustrated by the sample scenario considered in the simulations and calls for supplementary means of bridging data gaps of up to several minutes. Making use of the fact that the modified GPS receivers already provide the relative navigation solution in a co-moving RTN reference frame, the inter-satellite state vector can favorably be propagated over short time scales using Hill's equations [26]. The respective equations of motion allow for an analytic solution and are simple enough to be accommodated either inside the GPS receiver or the spacecraft's onboard computer. Further studies have therefore been initiated to assess the quality of this linearized relative motion model for short term propagation as well as editing and smoothing of the purely kinematic navigation solution.

Acknowledgements

Substantial work presented in this paper was performed during the first author's stay at the Center for Space Research, University of Texas (UT/CSR) within the visiting scientist program of the German Aerospace Establishment (DLR). The institutional and financial support received by these institutions is gratefully acknowledged.

References

[1] B.A.C. Ambrosius, E.T. Hesper, K.F. Wakker, Application of the Global Positioning System for Hermes Rendezvous Navigation, Journal of Guidance, Control and Dynamics 16 (1) (1993) 197–205.
[2] Arinc, ICD-GPS-200 Navstar GPS Space Segment/Navigation User Interfaces, Revison C, 25 Sept. 1997, Arinc Research Corp., El Segundo, 1997.
[3] P.W. Binning, I. Galysh, Satellite to satellite relative navigation using GPS pseudoranges, in: ION National Technical Meeting, Jan. 14–16, 1997, Santa Monica, 1997.
[4] W.H. Clohessy, R.S Wiltshire, Terminal guidance system for satellite rendezvous, Journal of Aerospace Science 270 (1960) 653.
[5] D.B. Cox, J.D.W. Brading, GPS autonomous relative navigation and time transfer for orbiting vehicles, in: ION GPS 95 Conference, Sept. 12–15, 1995, Palm Springs, 1995.
[6] T. Ebinuma, R.H. Bishop, E.G. Lightsey, Hardware-in-the-loop GPS test facility for spacecraft autonomous rendezvous, in: ION GPS 2001, Sept. 12–14, 2001, Salt Lake City, 2001.
[7] J. Galdos, T.N. Upadhyay, A GPS relative navigation filter for automatic rendezvous and capture, in: ION National Technical Meeting, Jan. 20–22, 1993, San Francisco, CA, 1993, pp. 83–94.
[8] F.R. Hoots, R.L. Roehrich, Models for propagation of NORAD element sets, Project Spacecraft Report No. 3, Aerospace Defense Command, United States Air Force, Dec. 1980.
[9] GEC, GPS Builder-2.1 12 Channel GPS Development System, DS4537, GEC Plessey Semiconductors, Issue 1.3.
[10] B. Hofmann-Wellenhof, H. Lichtenegger, J. Collins, Global Positioning System Theory and Applications, 4th Edition, Springer-Verlag, Wien, New York, 1997.
[11] J.L. Junkins, D.C. Hughes, K.P. Wazni, V. Pariypong, Vision-based navigation for rendezvous, docking and proximity operations, in: 22nd Annual AAS Guidance and Control Conference, Feb. 1999, AAS 99-021, 1999.
[12] E.D. Kaplan (Ed.), Understanding GPS Principles and Applications, Artech House Publishers, 1996.
[13] I. Kawano, M. Mokuno, T. Kasai, Relative GPS navigation for an automated rendezvous and docking test satellite ETS-VII, in: ION GPS 97, Sept. 16–19, Kansas, MO, 1997.
[14] Mitel, GPS Architect 12 Channel GPS Development System, DS4605, Mitel Semiconductor, Issue 2.5, March 1997.
[15] Mitel, GP2000 GPS Receiver Hardware Design, AN4855, Mitel Semiconductor, Issue 1.4, February 1999.
[16] O. Montenbruck, W. Enderle, M. Schesny, V. Gabosch, S. Ricken, P. Turner, Position-velocity aiding of a Mitel ORION receiver for sounding-rocket tracking, C5-5, in: ION GPS 2000 Conference, 19–22 Sept. 2000, Salt Lake City, 2000.
[17] O. Montenbruck, M. Markgraf, S. Leung, E. Gill, A GPS receiver for space applications, in: ION GPS 2001 Conference, 12–14 Sept. 2001, Salt Lake City, 2001.
[18] O. Montenbruck, E. Gill, Ionospheric correction for GPS tracking of LEO satellites, The Journal of Navigation 55 (2002) 293–304.
[19] O. Montenbruck, S. Leung, R. Bruninga, GPS operations on the PCsat microsatellite, in: ION-GPS-2002, Sept. 24–27, 2002, Portland, OR, 2002.
[20] S. Leung, Pulse Per Second (PPS) Implementation for the Mitel GPS Architect Receiver and Mitel Orion Receiver, DLR-GSOC TN 01-02, Deutsches Zentrum für Luft- und Raumfahrt, Oberpfaffenhofen, 2001.
[21] S. Leung, O. Montenbruck, B. Bruninga, Hot start of GPS receivers for LEO microsatellites, in: NAVITECH'2001, 10–12 Dec. 2001, Noordwijk, 2001.
[22] P.J.G. Teunissen, A. Kleusberg, GPS for Geodesy, 2nd Edition, Springer-Verlag, 1998.
[23] M.J. Unwin, M.K. Oldfield, C.I. Underwood, R. Harboe-Sorensen, The use of commercial technology for spaceborne GPS receiver design, in: ION-GPS-1998, Nashville, Sep. 15–18, 1998, p. 1983.

[24] M.J. Unwin, P.L. Palmer, Y. Hashida, C.I. Underwood, The SNAP-1 and Tsinghua-1 GPS formation flying experiment, in: ION GPS 2000 Conference, 19–22 Sept. 2000, Salt Lake City, 2000.
[25] A.J. Van Dierendonck, GPS receivers, in: J. Spilker, B. Parkinson (Eds.), Global Positioning System: Theory and Applications Vol. I, American Institute of Aeronautics and Astronautics, Washington, 1995, Chap. 8.
[26] D.A. Vallado, Fundamentals of Astrodynamics and Applications, McGraw-Hill, New York, 1997.
[27] P. Ward, Satellite signal acquisition and tracking, in: E.D. Kaplan (Ed.), Understanding GPS Principles and Applications, Artech House Publishers, 1996 (Chap. 5).
[28] G.G. Wawrzyniak, E.G. Lightsey, K.W. Key, J.W. Bell, M. Majka, R.S. Provence, Ground experimentation of a pseudolite-only method for the relative positioning of two spacecraft, in: ION GPS 2001, 11–14 Sept. 2001, Salt Lake City, 2001.